Non-Gaussian Dispersion in Model Smokestack Plumes

The dispersion of emissions from a plume in a cross stream was studied using both experimental and theoretical techniques. Wind tunnel experiments were done for three jet to cross stream velocity ratios: R = 0.5, 1, and 2. The concentration in the plane perpendicular to the cross stream was measured using light scattering and photographic image analysis. The analysis of the negatives revealed the presence of two counterrotating vortices that greatly affected dispersion of smoke in the plume.

Convection and random turbulent dispersion were modeled with a statistical convection simulator on a CYBER 205 computer. The input velocities to the convection model were obtained using experimental measurements. The model revealed the effects of the vortices on dispersion, and the concentration distributions across the plume were determined once the vortices had dissipated. The existence of the counterrotating vortices and their effects upon plume dispersion showed that the Gaussian plume model, which is widely used for modeling pollutant dispersion, is inapplicable in the near range of the model stack.

V. L. Thompson, R. A. Greenkorn
School of Chemical Engineering
Purdue University
West Lafayette, IN 47907

Introduction

The problem of modeling transport and dispersion of atmospheric pollutants is becoming more important as more contaminants are emitted into the atmosphere from coal-fired power plants. The general trend in atmospheric modeling has been to consider that emissions from a power plant follow a Gaussian distribution in the atmosphere, subject to deviations in wind direction and speed.

The major efforts thus far have been to develop dispersion models based on the assumption that turbulent dispersion is analogous to molecular diffusion, and can be represented by Fick's law. The Gaussian plume model, in which emission concentrations in the crosswind and vertical directions follow a Gaussian distribution, results from this assumption. However, the Gaussian model fails to account for the physical processes that are responsible for dispersion of emissions.

The Gaussian model arises from the solution to the advection-diffusion equation with semiinfinite boundary conditions. In most atmospheric dispersion models, an effective stack height is used to account for buoyancy of the plume. The concentration of an emission as predicted by the Gaussian plume model is:

$$C = \frac{Q}{2\pi\sigma_y\sigma_z u} \exp\left(\frac{-y^2}{2\sigma_y^2} + \frac{-z^2}{2\sigma_z^2}\right) \tag{1}$$

where:

C = emission concentration at a given x, y, and z
Q = source strength of a point source at $x = 0, y = 0, z$ = effective stack height
σ_y^2 = standard deviation of concentration in the y (crosswind) direction
σ_z^2 = standard deviation of concentration in the z (vertical) direction
u = wind velocity in the x (downwind) direction

The Gaussian model has many limitations. The model simplifies the complicated effects of uneven terrain, fluctuating winds, anisotropic or inhomogeneous turbulence, and unsteady source strengths. More important, the model neglects any crosswind or vertical velocities of the plume, which may greatly affect dispersion of pollutants emitted from the stack.

V. L. Thompson is currently with Exxon Production Research Company, Houston, TX 77098.

Possibly the most important mechanism for dispersion in the near range of the stack is dispersion caused by the turbulent vortices within the plume itself. While random turbulent motions can be accounted for by statistical means in the general Gaussian model, large-scale structured motions cannot be statistically represented. These large-scale plume vortices may dominate dispersion of power plant plumes as far downstream as 5 to 10 km.

To examine the velocity profiles of a plume in a steady cross flow, several investigators have performed experiments on a jet in a cross flow. As noted by Demuren (1983), Andreopoulos and Rodi (1984), Crabb et al. (1981), and Moussa et al. (1977), a plume in a steady cross flow can be modeled as a jet in a cross flow. With the advent of measurement techniques such as hot-wire anemometry and laser-Doppler velocimetry (LDV), experimental studies of jets in a cross stream have been greatly facilitated, and detailed quantitative data has been obtained.

One of the most extensive experimental studies of a round jet in a cross flow was performed by Andreopoulos and Rodi, who examined jet to cross flow velocity ratios of 0.5, 1.0, and 2.0 and determined three-dimensional velocity, kinetic energy, and shear stress profiles using a triple hot-wire probe. They described the existence of two counterrotating vortices generated on the lee side of the deflected jet, as well as a wake structure generated in the lee of the jet itself. The counterrotating vortices propagated downstream above the wake of the jet. The authors plotted the velocity vectors in the y (crosswind) and z (vertical) directions for various x distances downstream of the jet exit and clearly showed the rotating character of the flow field.

The motion of these bound vortices contradicts the assumption of negligible cross-stream and vertical velocities in the initial stages of the jet or plume, as the vortical motion induces transport of mass counter to the gradient. Thus as long as these counterrotating vortices persist in the flow, the plume will be non-Gaussian. As downstream convection continues, the vortical motion dissipates or the vortices may coalesce. In this region the crosswind dispersion will undergo a transition from a mechanism that is dominated by the convection due to the vortices to a mechanism that is dominated by the random turbulent motion in the plume. Under random turbulence dominated dispersion, the convection in the cross-stream and vertical directions due to the vortices is no longer important, and the plume will eventually become Gaussian. The problem then becomes one of defining the vortical motions of these counterrotating structures, determining how long they persist, and determining when the Gaussian plume model, which assumes a point source with no convection in the crosswind and vertical directions, is valid.

Statistical Convection Simulator

A simulation model was developed that accounts for crosswind convection and a statistical representation of random turbulent dispersion. This statistical convection simulator (SCS) was originally developed to handle dispersion and one-dimensional convection by Ahlstrom et al. (1977). The model can trace fluid particles through a given flow field and has been modified to cover three-dimensional convection. This model was implemented by Cala and Greenkorn (1982) for calculating dispersion during flow through heterogeneous porous media.

The model contains two steps: a convective motion and a dispersive motion. The fluid particles travel through the flow field by increments of time, which can be obtained from the downstream velocity (x direction) divided by the distance traveled. The convective motion is described by the following equations (for a two-dimensional flow field):

$$y_i = y_{i-1} + v_y \Delta t \tag{2}$$

$$z_i = z_{i-1} + v_z \Delta t \tag{3}$$

where y_i, $z_i = y_i$ and z are coordinates of the fluid particle at step i, and v_y = crosswind component of velocity, v_z = vertical component of velocity, Δt = time increment.

On the microscopic level, the dispersion step represents random turbulent dispersion. This dispersion, as described by Ahlstrom et al. and Cala and Greenkorn, can be modeled as a random walk process. The particles are assumed to diffuse with a Brownian-like motion:

$$y_i = y_{i-1} + y' \tag{4}$$

$$z_i = z_{i-1} + z' \tag{5}$$

The root mean square distance moved in a time step Δt is:

$$d_{RMS} = \sqrt{2\Delta t K} \tag{6}$$

where K is the turbulent dispersion coefficient.

The deviation from y_i, y', is:

$$y' = [R]_{+\xi}^{-\xi} \tag{7}$$

where R is a random number from $-\xi$ to $+\xi$.

The model can be used to generate concentration profiles in a jet in a cross flow and determine the mixing of the emissions in this manner. By inputting the v and w velocity profiles for different x locations (time steps) as measured by Andreopoulos and Rodi, the effect of the counterrotating vortices on plume dispersion is evident. It is important to note that the v and w velocities will change with distance downstream from the jet exit, and the vortices will eventually die out, as indicated by the measurements of Andreopoulos and Rodi. However, it has been observed experimentally that although the velocities themselves die out, the shape of the jet and the distribution of concentration in the jet remains non-Gaussian for some time downstream of the jet exit. This effect is also seen in the SCS model using the input of the experimentally measured velocities for the y (crosswind) and z (vertical) directions. These velocities were used to determine dispersion in a jet in a cross stream with the SCS model.

Experiments

The experimental wind tunnel setup is shown in Figure 1. A front-surface mirror was attached to the end of an 11.5 in. (29.2 cm) arm that was secured to a synchronous motor. An argon ion laser operated at a power of 0.8 W was directed toward the mirror and focused with a series of lenses so that the beam passing through the smoke was as small as possible. The aerosol smoke was generated using a TSI atomizer, which generates monodisperse aerosols from a kerosene liquid in air. The particles, also used for LDV measurements, were from 1 to 2 μm in diameter. The flow rate of air through the atomizer was kept constant for

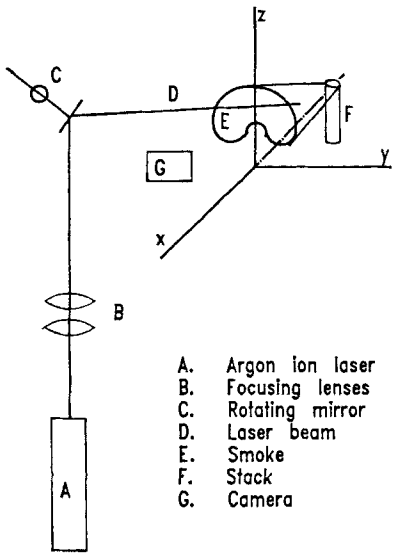

Figure 1. Diagram of experimental apparatus.

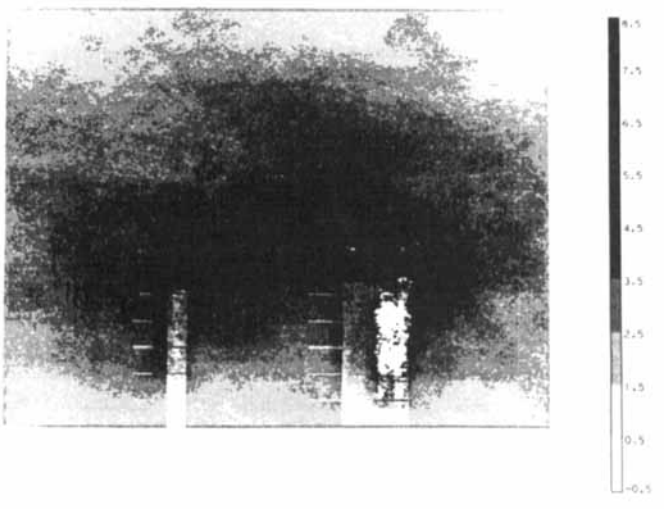

Figure 2. Ensemble average relative concentration distribution.
$R = 0.5$; $x/D = 1.0$; $Re = 20{,}930$
Background scattering from model stack has been subtracted

each set of experiments in order to provide a constant jet velocity. The particles were neutrally buoyant and were released into a neutrally stable flow in the wind tunnel.

The beam passed through 5° in 0.0347 s to freeze the macroscale motions. A 35 mm camera was set up parallel to the beam (parallel to the y-z plane of the smoke) so that the image of the y-z plane of the smoke could be captured on film. The shutter was manually opened and shut after each pass by the beam through the smoke. Kodak black-and-white Tri-X 150 400 film was used to photograph the image.

Three different model stack sizes were used. In order to duplicate the experiments of Andreopoulos and Rodi and thus compare the results of the experiments with the concentration distributions obtained from the SCS model using their data, a stack 5 cm in dia. was placed in the wind tunnel. This stack was operated at an exit velocity of 6.3 m/s, while the tunnel was operated at 12.6 m/s, for a value of $R = 0.5$, where R is the ratio of stack exit velocity to downstream velocity. It was decided to scale down the experiments to lower tunnel velocities in addition, because the tunnel velocity became more erratic at higher velocities. Table 1 lists the experiments performed.

The negatives were analyzed for gray levels using an E. Leitz image analyzer. The image was divided into 256 × 256 points (pixels) on a screen. The image analyzer indicates all pixels at a given gray level. A composite image was made using a false-color representation of each of ten gray levels, and the gray level images were averaged to give an ensemble average image of the y-z plane.

Table 1. Experiments

	Velocity, m/s		
R	Stack Exit	Cross Flow	Re
0.5	6.3	12.6	20,930
0.5	3.2	6.3	5,316
1.0	7.2	7.2	11,960
2.0	8.9	4.5	14,784

Results

For the case where $R = 0.5$, two sets of experiments were performed. The first set of experiments was a re-creation of the experiments performed by Andreopoulos and Rodi, in order to obtain concentration data to correspond with their measured velocities used in the theoretical calculations. The second set of experiments was performed at a lower Re (with lower velocities) in order to compare with the first set of experiments and thus analyze the data obtained for $R = 1.0$ and $R = 2.0$.

Figures 2 and 3 are the ensemble average images of the smoke at a downstream distance of one stack diameter. The corresponding calculation made for this case is shown in Figure 4. Figure 4 illustrates the comparison between measured relative concentration and the calculated relative concentration from the SCS model. The concentrations were normalized by setting the highest measured or predicted concentration to 1.0, and the lowest concentration to 0.0, for both the experimentally measured

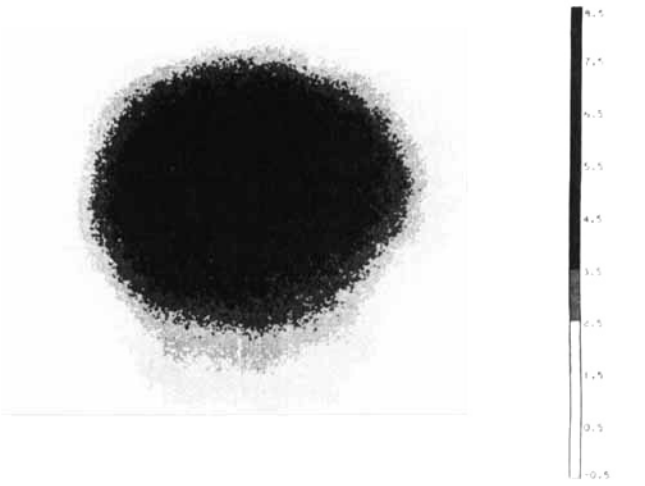

Figure 3. Ensemble average relative concentration distribution.
$R = 0.5$; $x/D = 1.0$; $Re = 5{,}316$

concentrations and the SCS model predictions. Figure 2 is the experiment that replicated the experiments of Andreopoulos and Rodi, and Figure 3 is the experiment performed at a lower *Re* with a stack diameter of 1 in. (25.4 mm). The background, which showed the stack area, has been removed from Figure 2.

The differences between Figure 2, taken at one stack diameter downstream at a *Re* of 20,930, and Figure 3, also at one stack diameter but at a lower *Re* of 5,316, are obvious. The most striking difference between the pictures is that the kidney shape is very evident in the experiments performed at a higher *Re*, while the experiments at *Re* = 5,316 show a Gaussian profile with an area at the bottom of the jet that appears to trail downward. This is most likely due to entrainment in the wake behind the stack, as described by Andreopoulis and Rodi. This wake may have obscured the vortices for the lower *Re*. The main conclusion that can be drawn from this comparison is that at higher *Re* the vortices may be even more pronounced. The values of the velocities are greater in the vortices for a higher *Re*, and thus the vortices will dissipate more slowly.

Figure 4 illustrates the comparison between measured and predicted relative concentrations at different vertical levels (z/D). The concentrations in Figure 4 were normalized by setting the highest measured or predicted concentration to a value of 1.0 and the lowest concentration to 0.0, for both the experimentally measured relative concentration and the SCS prediction of relative concentration. As seen in Figure 4, the model predicts the kidney shape of the vortices to begin at a greater z/D than actually seen. The model does not predict the Gaussian distribution at $z/D = 2.625$, but rather a concentration distribution with three peaks. This can be attributed to two causes:

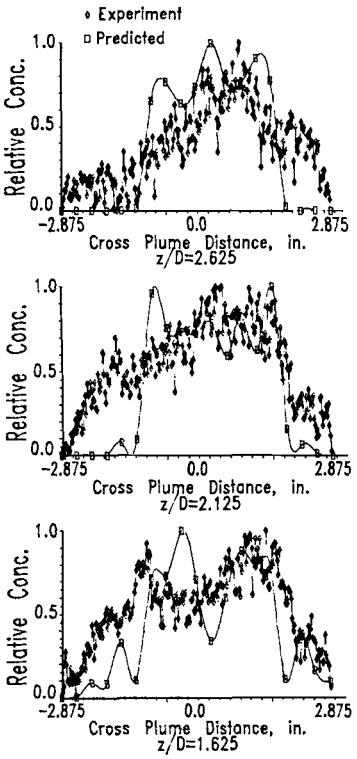

Figure 4. Measured and predicted relative concentrations.
$R = 0.5$; $x/D = 1.0$; $Re = 20{,}930$

First, the measurements of Andreopoulos and Rodi used in the SCS model prediction gave values of y and z velocities at the top of the plume that were not insignificant. Second, the experimentally measured velocities at the center of the plume were very low, and thus the fluid particles that move to the center of the plume or begin at the center are mainly subject to movement by random dispersion rather than convection, and therefore remain at the center, causing a peak to appear in the predicted concentrations.

The jet spreads out in the horizontal and vertical directions as it travels downstream due to both convection and dispersion. The Andreopoulos and Rodi velocity measurements for v and w velocities to ten stack diameters were used in the SCS model for the convection step. Beyond ten stack diameters downstream (in the x direction), it was assumed that these velocities had dissipated. The kidney shape of the jet was still evident at 20 stack diameters downstream for the model predictions of relative concentration distribution. Thus for $R = 0.5$, the model predicts that the plume will be non-Gaussian at least as far downstream as 20 stack diameters, even though random turbulent dispersion is the dominant dispersion mechanism beyond ten stack diameters downstream.

Figure 5 is the ensemble average of negatives taken with a jet to cross flow ratio of 1.0 at a distance of four stack diameters downstream. The corresponding comparison of experimental measurements and calculated relative concentrations made with the SCS model is shown in Figure 6.

A comparison between Figure 5 and Figure 6 shows the striking vortices seen at $R = 1.0$. The experiments indicate a Gaussian profile across the top of the jet, with a tendency to become non-Gaussian as the vortices influence the flow at the bottom of the jet. These vortices begin to appear at $z/D = 3.8$. Once again, a concentration peak at the centerline is predicted by the model due to the velocity minima reported at that line. However, agreement between predicted and measured peaks resulting from the vortex motion appears to be quite good. The kidney shape of the jet is evident in both the SCS calculations and the experimental measurements.

Model calculations were performed from two to 200 stack diameters downstream from the jet exit. The kidney shape of the

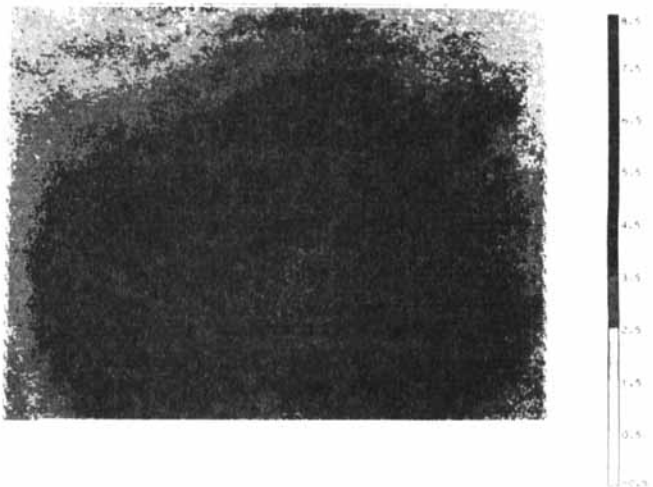

Figure 5. Ensemble average relative concentration distribution.
$R = 1.0$; $x/D = 4.0$; $Re = 11{,}960$

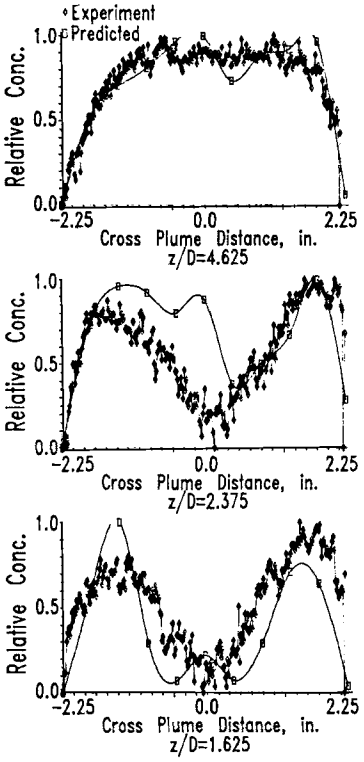

Figure 6. Measured and predicted relative concentrations.
$R = 1.0$; $x/D = 4.0$; $Re = 11{,}960$

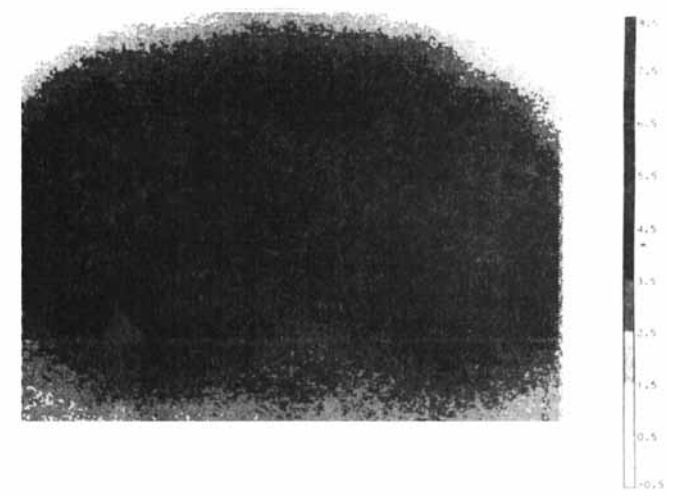

Figure 7. Ensemble average relative concentration distribution.
$R = 2.0$; $x/D = 4.0$; $Re = 14{,}784$

jet persisted until approximately 40 stack diameters. The calculations carried out to 100 and 200 stack diameters were influenced solely by random turbulent dispersion and at 200 stack diameters in the x direction the jet had assumed a Gaussian profile.

The ensemble average for a jet to cross flow ratio of 2.0 at four stack diameters downstream is shown in Figure 7. The corresponding comparison between experimental relative concentrations and SCS calculations for $R = 2.0$ is shown in Figure 8. Both again show a marked kidney shape to the jet. The SCS model calculations of concentration for $R = 2.0$ were also carried out to 200 stack diameters downstream. While the concentration peaks due to the vortical motion began to dissipate by $x/D = 100$ for $R = 1.0$, the kidney shape of the jet was still evident at $x/D = 200$ for $R = 2.0$. This can be attributed to the greater velocity values in the vertical and horizonal directions, and the greater distance of propagation of the velocities for $R = 2.0$.

The Peclet number, Pe, is defined as the ratio of convective forces to diffusive forces, $Pe = \nu/\Gamma$, where ν is the diffusivity due to convection and Γ is the diffusivity due to random dispersion.

It might appear that below a certain Peclet number, that is, when convection is much lower than dispersion, the plume assumes a Gaussian distribution. Although convection is no longer the dominating influence on plume dispersion when $Pe < 1$, the effects of the convective motion of the counterrotating vortices persist. Due to the influence of the vortices at the outset, the plume has dispersed in a non-Gaussian manner until the vortices have dissipated. With the plume now possessing a non-Gaussian distribution, the main dispersive mechanism in the crosswind plane becomes the random turbulent motions, which are described by a statistically derived dispersion coefficient. There is a time lag during which the plume remains non-Gaussian even though convective motion is not dominating dispersion. This constitutes a transition period beginning at $Pe = 1$ and ending when the plume has dispersed randomly so that it becomes describable by statistical means. For each case of jet to cross stream ratios, the downstream distance from the point

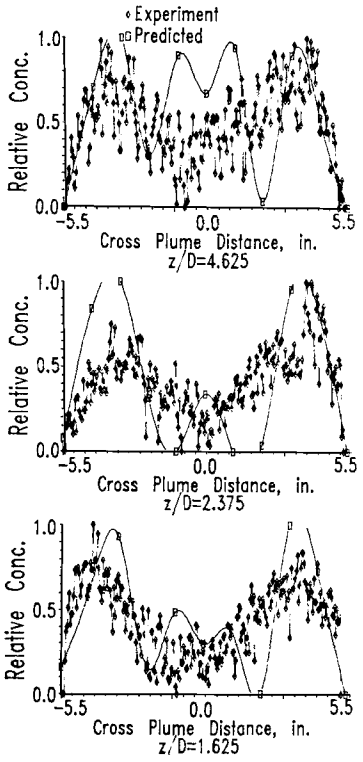

Figure 8. Measured and predicted relative concentrations.
$R = 2.0$; $x/D = 4.0$; $Re = 14{,}784$

where $Pe < 1$ to the point where the plume appears to be Gaussian increases with increasing R.

Summary and Conclusions

A statistical convection simulator model was developed to describe flow in a jet in a cross stream. The jet in a cross-stream model can be extended to the study of a plume in the atmospheric boundary layer under the influence of neutral buoyancy and steady wind. The trends shown by the model agreed with the ensemble-averaged concentration profiles measured by image analysis of negatives taken in a wind tunnel model. The SCS model indicates, in agreement with experimental data, that the most important parameter in determining the strength and length of the propagation of the vortices is R, the jet to cross flow ratio.

A comparison of jet structure at two different Reynolds numbers, Re = 20,930 and 5,316, indicates that the higher the Re, the stronger the vortex motion. This can be explained by the higher momentum possessed by the jet as it leaves the stack. The vortices generated at a higher Re will propagate farther downstream as well. Thus in applications to a power plant plume where a typical Re is on the order of 10^6, the bound vortices will influence the flow field even farther than in the tunnel experiments performed at an Re of 10^4.

The statistical convection simulator predicts the resultant kidney shape of the jet using experimentally measured v and w velocities as input. The model agreed well with the trends shown in the experiments for peak and low concentrations, except at the centerline of the jet, where the SCS model erroneously predicts a concentration peak. This was due to the low values of velocity at the centerline used in the model calculations. The model also shows a skewness, which is unexpected for a symmetric jet. This is again explainable by the use of data with negative velocities in the crosswind (y) direction at the jet centerline.

The SCS model predicts that the kidney shape caused by the presence of the vortices carried out through 20 stack diameters downstream of the jet exit for the case where the jet to cross stream ratio is 0.5. For R = 1.0 the vortex structure appears to die out at 100 stack diameters, resulting in a Gaussian profile at 200 stack diameters. For the case where R = 2.0, the kidney shape is still highly visible even at 200 stack diameters. For a typical power plant plume, this translates to more than 1 km downstream of the stack that the vortices still influence the dispersion of gases. While the Gaussian model, which is typically used to model atmospheric dispersion from power plant plumes, assumes that a plume is a point source and that dispersion proceeds according to random motion from that point source, this is incorrect in the near range of the stack exit. However, as long as the kidney-shaped configuration of the plume persists due to convection-dominated dispersion from the stack exit, the point source assumption of the Gaussian plume model is inaccurate. Thus at R = 2.0, at least as far from the stack exit as 200 stack diameters the Gaussian plume model yields an erroneous concentration distribution. A more accurate model might begin with a simulation of plume dispersion such as the one described in the SCS model, which would then provide concentration distributions for the Gaussian plume model farther downstream of the stack exit, thus providing a more physically realistic source term.

The SCS model also provides some improvement in time requirements for a calculation of concentration distribution. Given a velocity distribution and a statistical representation of dispersion, the model provides a simplified calculation for concentration over the solution of the three-dimensional turbulent momentum equations coupled with the equation of continuity for concentration distribution. The velocity distribution could be obtained either by experiment, as illustrated, or by solving the momentum equations by a numerical technique.

A quantitative comparison between the measured concentration would lead to the conclusion that the model overpredicts peak concentrations. This, then, would have the consequence of overpredicting the non-Gaussian region in the plume. However, it must be pointed out that no attempt was made to quantify relative concentration. In order to gain an accurate quantitative comparison between model predictions and experimental measurements, it will be necessary to measure absolute concentrations.

Acknowledgments

This work was supported by the Purdue University Coal Research Center through a grant from the Conoco Coal Company. We thank J. P. Sullivan of the Purdue School of Aeronautics and Astronautics for his advice and support.

Notation

C = emission concentration in Gaussian plume model
D = stack diameter
d_{RMS} = root mean time step traveled in time increment
K = turbulent dispersion coefficient
Pe = Peclet number
Q = source strength of a point source in Gaussian plume model
R = jet to cross-flow velocity ratio
Re = Reynolds number
Δt = time increment
u = wind velocity in x (downwind) direction
v_y = crosswind component of velocity
v_z = vertical component of velocity
y_i = crosswind position of fluid particle at step i
y' = random fluctuation of fluid particle from crosswind position
z_i = vertical position of fluid particle at step i
z' = random fluctuation of fluid particle from vertical position

Greek letters

Γ = diffusivity due to random dispersion
$-\xi, +\xi$ = limits on random number
ν = diffusivity due to convection
σ_y^2 = standard deviation of concentration in y (crosswind) direction
σ_z^2 = standard deviation of concentration in z (vertical) direction

Literature Cited

Ahlstrom, S. W., H. P. Foote, R. C. Arnett, C. P. Cole, and R. J. Serne, "Multicomponent Mass Transport Model: Theory and Numerical Implementation (Discrete-Parcel–Random-Walk Version)," BNWL-2127, Battelle Pacific Northwest Labs (1977).

Andreopoulos, J., and W. Rodi, "Experimental Investigation of Jets in a Crossflow," *J. Fluid Mech.*, **138,** 93 (1984).

Cala, M. A., and R. A. Greenkorn, "Velocity Effects on Dispersion in Porous Media with a Single Heterogeneity," *Water Resour. Res.*, **22**(6), 919 (1982).

Crabb, D., D. F. G. Durao, and J. H. Whitelaw, "A Round Jet Normal to a Crossflow," *Trans. ASME,* **103,** 142 (1981).

Demuren, A. O., "Numerical Calculations of Steady Three-dimensional Turbulent Jets in Cross Flow," *Comput. Meth. Appl. Mech. Eng.*, **37,** 309 (1983).

Moussa, Z. M., J. W. Trischka, and S. Eskinazi, "The Near Field in the Mixing of a Round Jet with a Cross Stream," *J. Fluid Mech.*, **80,** 49 (1977).

Manuscript received Mar. 10, 1987, and revision received Aug. 5, 1987.